TÜBİTAK

Turkish Journal of Chemistry

http://journals.tubitak.gov.tr/chem/

Research Article

Turk J Chem
(2022) 46: 415-433

doi:10.3906/kim-2106-55

Cerium and europium doped TiO_2 thin films deposited by a sol-gel dip-coating process: characterization and photocatalytic activity toward dye degradation

Dalanda HAMDI[1,2], Lobna MANSOURI[1], Varsha SRIVASTAVA[3], Mika SILLANPAA[4,5], Latifa BOUSSELMI[1,*]

[1]Laboratory of Wastewater and Environment, Center for Water Research and Technologies of BorjCedria Tunisia (CERTE), Technopark Borj Cedria, Soliman, Tunisia

[2]University of Gabes, National school of engineers of Gabes, Gabes, Tunisia

[3]Research Unit of Sustainable Chemistry, Faculty of Technology, University of Oulu, Oulu, Finland

[4]Environmental Engineering and Management Research Group, Ton Duc Thang University, Ho Chi Minh City, Vietnam

[5]Faculty of Environment and Labour Safety, Ton Duc Thang University, Ho Chi Minh City, Vietnam

Received: 25.06.2021 • **Accepted/Published Online:** 01.12.2021 • **Final Version:** 27.04.2022

Abstract: Cerium (Ce) and europium (Eu)-doped TiO_2 thin films were obtained by sol-gel dip-coating technique. SEM micrographs showed that the surfaces are covered by agglomerated particles due to the repeating coating process. XRD patterns showed the presence of TiO_2 anatase phase. Raman spectra revealed that the peaks recorded at 146 cm^{-1}(E_g) and 397 cm^{-1}(B_{1g}) were related to the anatase phase. EIS measurements proved that Ce-TiO_2 (1wt%) and Eu-TiO_2 (0.1wt%) photocatalysts possessed a lower electron transfer resistance than pure TiO_2, which can lead to effective separation of electron/ hole pairs during the photoreactions. The photoactivity of Ce and Eu-doped TiO_2 was investigated by the degradation of amido black10B dye (AB) under UV excitation and varying the initial pH and concentrations. It was found that Eu-TiO_2 (0.1wt%) exhibited higher photocatalytic activity, reaching a first-order reaction rate of k_{app} (0.036min^{-1}), $t_{1/2}$ was around 12 min and AB removal was 98.94%, under optimal pH of 3.5 and AB concentration of 10ppm compared to ($t_{1/2}$= 45 min, $t_{1/2}$=30 min), (k_{app}= 0.022 min^{-1}, k_{app}=0.026min^{-1}) and AB removal (94.78%, 96.44%), respectively for pure TiO_2 and Ce-TiO_2 (1wt%). Further increase in Eu/Ce amount up to optimal concentration (1wt% Ce and 0.1wt% Eu) led to a decrease in the AB removal. The mineralization of AB using Eu-TiO_2 photocatalyst was confirmed by HPLC analysis.

Key words: TiO_2, cerium, europium, sol-gel, dip coating, silicon, photodegradation

1. Introduction

TiO_2 catalyst has been proven to be the widely used material in several applications [1,2]. Due to its multi-faceted functional properties, TiO_2 is known as a promising photocatalyst material generally used in photocatalytic reactions for water treatment process [3]. Besides its strong mechanical properties, TiO_2 has received considerable attention as it is inexpensive, chemically stable, nontoxic, and with great oxidation ability [4]. However, anatase TiO_2 is a material with wide band gap (Eg = 3.23eV) that exhibits recombination of electron/hole pairs [5]. Thereby, several researchers have modified TiO_2 nanomaterials using rare earth elements (RE) such as Ce, La, and Er to enhance the photocatalytic activity under UV irradiation [6,7]. Among them, Ce ions have strong absorption ability and showed efficient optical properties to improve the photocatalytic efficiency of TiO_2 photocatalyst [8]. In fact, Ce ions can enhance the efficiency of the photodegradation via inhibiting the recombination rate of photogenerated electron/ hole pairs by acting as electron traps [9]. Furthermore, Ce ions have been reported to shift the band edge in TiO_2 to the visible region and improve the redox potential of the photo-generated radicals [7,10]. On the other hand, Eu ions doping has attracted much attention in photocatalytic process due to its higher photocatalytic activity than pure TiO_2 in the degradation of organic pollutants [11]. Thereby, recent studies have reported the photocatalytic enhancement of RE-doped TiO_2 thin films [9,12,13,14,15,16,17,18,19]. TiO_2 photocatalyst can be used in slurry or immobilized systems [20]. However, in a slurry system the separation step of the catalyst particles constitutes a major drawback, and it is needed to avoid as it is costly, unless it remains mandatory [21]. Thereby, the photocatalytic oxidation using an immobilized TiO_2 photocatalyst is more recommended [22]. Silicon (Si) is a semiconductor with a narrow indirect band gap (1.12 eV) [23]. p-Si was used as photocatalyst substrate [24], because its abundant and eco-friendly [25]. Therefore, Si is an encouraging material for making eco-friendly and visible-

* Correspondence: latifa.bousselmi@certe.rnrt.tn

light active photocatalyst-based heterostructures. p-Si used as substrate was reported to show an enhancement in the photocatalytic activity of n-photocatalyst compared to the glass substrate [26]. This enhancement in photocatalytic activity can be explained by the contribution of the inner electric field of the p-Si/ n-TiO_2 heterojunction to the separation of photogenerated electron/ hole pairs. Thereby, when photons of the p/ n heterojunction are irradiated with energies equal or higher than the band gaps of n-TiO_2 and p-Si, electron/ hole pairs are generated. Due to the action of the inner electric field, the photogenerated electrons can be injected from the conduction band of p-Si to that of n-TiO_2. In the valence band, the photogenerated holes migrate in the reverse direction [27,28]. Subsequently, the photogenerated electrons in the n-TiO_2 conduction band can be trapped by the adsorbed O_2 molecules to produce superoxide radical anions, and the photogenerated holes in p-Si valence band can be scavenged by the H_2O molecules to produce •OH that are responsible for degradation of organic molecules. Therefore, the photogenerated electrons and holes are efficiently separated and the recombination of electron/ hole pairs is suppressed, and the photocatalytic activity is enhanced. For these reasons, various methods have reported the synthesis of TiO_2 thin films such as: chemical vapor deposition (CVD) [29,30], atomic layer deposition [31,32,33], electrochemical anodization [34] and sol-gel process [35,36]. Particularly, the sol-gel technique involves thin film depositions with a large specific surface area, high purity and mechanical resistance, good crystallinity, chemical durability, and controlled conditions of morphology, composition, and thickness [37,38]. Among sol-gel process, the dip-coating technique is used for immobilization purposes in a wide range of applications [39,40]. The dip-coating process is an economically feasible technique. It can be carried out at room temperature, and applied to a wide variety of substrates with large surfaces and various form [41]. The dip-coating process can produce films with high uniformity and a thickness ranging from nanometers to 200 nm for oxide films [42]. The good uniformity of the thin films obtained by dip-coating technique can be reached due to the layer-by-layer growth during each dip process of the substrate in the precursor solution [43]. The sol-gel dip-coating technique is essentially based on mechanisms of hydrolysis and polycondensation of titanium alkoxides mixed with alcohol and catalytic agents [35,44].

In the present study, Ce or Eu doped-TiO_2 thin films are coated on both sides, by the sol-gel dip coating process, on p-silicon wafers (p-Si). The effect of dopant ions on the structural, morphological properties and photocatalytic activity under UV irradiation are discussed in details. Amido black 10B dye was selected, as a model pollutant, to test the photocatalytic activity of this new synthesized materials, under different operational conditions (initial pH value (3.5, 5.5, 7, and 9), dye concentration (10, 20, 30, and 40 ppm). The photo-electrochemical behavior of the pure and doped TiO_2 electrodes was carried out by the measurements of the electrochemical impedance spectroscopy (EIS) in the dark before and after UV irradiation in alkaline medium.

2. Experimental

2.1. Reagents

Titanium (IV) isopropoxide ($C_{12}H_{28}O_4Ti$; CAS Number 546-68-9; purity: 97 %), acetic acid (≥99.5%), Amido Black 10B ($C_{22}H_{14}N_6Na_2O_9S_2$), and absolute ethanol (99.98%) were used without purification and were purchased from Sigma Aldrich. Cerium (III) nitrate hexahydrate (99% trace metal basis) and europium (III) nitrate pentahydrate (99.9%) were obtained from Aldrich Chemistry. Hydrofluoric acid (40% purity) was acquired from Emsure. Sodium hydroxide was purchased from Sigma Aldrich. All solutions were prepared using ultrapure water (18.2 MΩ) produced in a Direct-Q millipore system. Silicon wafers (CAS Number 7440-21-3) p-type (100) were provided by Si-Mat silicon materials, Germany.

2.2. Synthesis and coating of Ce and Eu doped TiO_2 thin films on p-silicon wafers

In the present study, pure and doped TiO_2 thin films were cast by the dip-coating process using of titanium (IV) isopropoxide as a precursor of TiO_2. Pure, Ce, and Eu doped TiO_2 thin films were coated, on p-silicon wafers on both sides, using a HOLMARC's dip coating unit with the infrared dryer (HO-TH-02B). Firstly, 18 mL of titanium (IV) isopropoxide was dissolved in 100 mL of ethanol and stirred for 30 min, then 3 mL of acetic acid was added dropwise and the mixture was stirred again for 5 h. When required, different atomic weight percentages of Ce $(NO_3)_3$ (Ce: 0.1, 0.5, 1, 3, and 5wt%) or $EuH_{10}N_3O_{14}$ (Eu: 0.1, 0.5, and 1wt%) were added to the mixture, respectively, for the synthesis of Ce-TiO_2 and Eu-TiO_2 films. The substrates were immersed in the titanium precursor solution for 2 min and withdrew at a constant speed of 5mm.s^{-1} to deposit one layer of the film. After each dip process, the samples were automatically dried at 100 °C for 10 min, to evaporate the solvent. The process of dip-drying was repeated five times. Then, the prepared thin films were annealed at 500 °C by heating at a defined rate, for 2h. It is necessary to report that prior to deposition, the rectangular p-Si substrates (10.5cm^2) were cleaned with hydrofluoric acid and ethanol, then rinsed with deionised water and finally dried in order to remove native oxide.

2.3. Analytical methods

-Structure and morphology: The morphological properties of pure TiO_2, Ce-TiO_2, and Eu-TiO_2 thin films were studied by means of SEM-EDS microscope (Hitachi S-4800 Ultra-High Resolution Scanning Electron Microscope High-Resolution Field-Emission scanning electron microscope (SEM)) having a resolution of 1nm. The crystalline structure analysis of the samples was studied using X-ray diffraction radiation (XRD) analysis using XRD PANalytical Empyrean. Raman spectra were investigated on a JYT64000 Raman spectrometer Horiba Jobin Yvon, Labram HR at green laser (514.53 nm).

-Photoelectrochemical and electrochemical measurements: They were performed in 0.1M NaOH at room temperature using three-electrode cell quartz (100 mL), where the elaborated materials, served as working electrodes, a platinium eletrode served as counter-electrode. All potentials were measured and referred to a saturated calomel reference electrode (SCE). Photoelectrochemical characterization were performed using a VoltaLab 40 PGZ301 potentiostat (Radiometer Analytical), connected with a computer that uses VoltaMaster 4.0 software for data acquisition. EIS measurements were carriedout with 10 mV applied sinusoidal AC perturbation over the frequency range of 0.125-10^5 Hz. Photopotential (Eocp) measurements of the electrodes were carried out when no bias is applied to the photoelectrode, during on/off cycle of UV irradiation, provided by a high pressure mercury lamp (Cathodeon HPK 27.5 mW; λ = 365.5nm), exposed to one-coated side of the eletrodes. Data were recorded and fitted with Z-Simpwin 3.2 software. Photoelectrochemical measurements were performed in NaOH(0.1M) at room temperature using three-electrode quartz (100 mL), where the Ce-TiO_2 (1wt%) and Eu-TiO_2 (0.1wt%) (obtained under optimised conditions) and pure TiO_2 photocatalyst, served as working electrodes. All potentials were measured and referred to a saturated calomel reference electrode (SCE). Photoelectrochemical characterization was performed using a VoltaLab 40 PGZ301 potentiostat (Radiometer Analytical), with VoltaMaster 4.0 software for data acquisition.

-Technical analysis: The HPLC spectra were recorded on an Agilent 1260 Infinity II liquid chromatography system with diode array detector (DAD, Agilent G1315D) set as 254nm. The chromatographic conditions were: mobile phase 60%v methanol: 40%v water, flow rate 1mL.min^{-1}, injection volume 20 µL, chromatographic column LC18 column Zorbax ecli pse XDB (250×4.6 mm). UV-Visible spectra and analytical determination of AB remaining in solution were done calorimetrically (620nm) using UV-Vis spectrophotometer (Perken Elmer Lampda 450) and HPLC system with diode array detector (DAD, Agilent G1315D) set as 254nm.

2.4. Photodegradation experiments

The photocatalytic performance of the synthesized Ce-TiO_2 and Eu- TiO_2 thin films was evaluated by studying the discoloration of amido black dye solution as a model pollutant under UV light. The photodegradation experiments were carried out in a quartz beaker, equipped with a magnetic stirring bar. The UV irradiation was provided by two replacement tubes (HITACHI, shortwave 254nm) placed on parallel, in a way to effectively illuminate both coated surface sides. The synthesized Ce-TiO_2 and Eu- TiO_2 supported on silicon wafers were immersed in 50 mL of AB dye aqueous solution. The distance between the AB dye solutions and the UV light source was fixed to 10 cm, from both sides. During the different photocatalytic experiments, several operational parameters (AB concentration, pH, and type of the used catalyst), were varied to study their effects on pollutant degradation. The initial pH of AB aqueous solutions was adjusted prior to each experiment by NaOH or HCl solutions (0.1M).

3. Results and discussion

3.1. SEM-EDS analysis

Figure 1 shows examples of SEM patterns (top views) of the undoped and Ce or Eu- doped TiO_2 films deposited on silicon wafers by sol-gel dip-coating technique (optimal photodegradation results). Figure 1 shows SEM images of annealed pure and doped-TiO_2 thin films. The pure TiO_2 sample seems to have a smooth surface without any cracks (Figure 1a). After Ce and Eu doping, the surfaces showed agglomerated particles for Ce-TiO_2 and Eu-TiO_2 samples. Thus, despite the absence of cracks and fissures as clearly shown by SEM analysis (Figure 1b and 1c), there is no doubt that the coating process repeated 5 times affected the agglomeration of the particles after adding dopant ions. In fact, the addition of Ce and Eu ions generated oxygen vacancies, as confirmed by Raman analysis (shift in E_g mode to higher wavenumber). The larger ionic radius of Ce^{3+} (0.111 nm) and Eu^{3+}(0.095 nm) compared to Ti^{4+}(0.068 nm) ions, make the Ce^{3+}/ Eu^{3+} ions unable to substitute Ti^{4+} in the TiO_2 lattice. The oxygen vacancy defects in case of Ce/Eu-doping generate a charge decompensation favoring the agglomeration process [45].

The average film thickness of the layers obtained from the cross-section (not shown here) is illustrated in Table 1. It is about 6.4 µm for pure TiO_2 thin film. However, doping TiO_2 thin film with Ce led to a decrease in film thickness up to 4.5, 4.1, 2.7, 1.4µm, respectively for (Ce: 0.1, 0.5, 1, 3 wt%), then increased again to 3.7 µm for Ce (5wt%). However, when TiO_2 thin film is doped with Eu, the film thickness decreased up to 2.7 µm and 1.4µm, respectively for (Eu: 0.1 and 0.5 wt%),

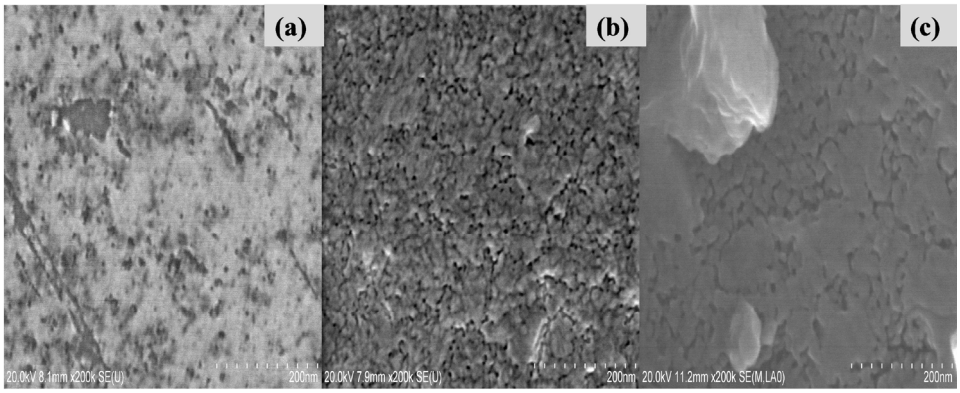

Figure 1. SEM analysis of (a) Pure-TiO_2, (b) Ce-doped TiO_2, and (c) Eu-doped TiO_2 thin films.

Table 1. Effect of different Ce and Eu content on thickness of the prepared TiO_2 doped thin films, and atomic ratio Ce/Ti and Eu/Ti.

Sample	Thickness (μm)	Ce/Ti and Eu/Ti atomic ratio
Pure TiO_2	6.4	0
0.1wt% Ce-TiO_2	4.5	0.1
0.5wt% Ce-TiO_2	4.1	0.5
1wt%Ce-TiO_2	2.7	0.8
3wt%Ce-TiO_2	1.4	1.3
5wt%Ce-TiO_2	3.7	2.2
0.1wt% Eu-TiO_2	2.7	0.1
0.5wt% Eu-TiO_2	1.4	0.1
1wt% Eu-TiO_2	2.7	0.4

then increased again to 2.7 μm for Eu (1wt%) (Table 1). This behavior is linked to the fact that increasing gradually dopant concentration in the solution retards the growth of TiO_2 thin film [46]. According to these results, the film thickness of pure TiO_2 thin film prepared by sol-gel dip-coating technique in the present study is higher (6.4 μm) than that prepared by sol-gel spin-coating technique as reported by [47] (3.8 μm) in the same conditions of sol precursor solution and after five times coating. In fact, dip-coating technique requires the immersion of a substrate in titanium precursor in a volume solution of 50 mL and the spin coating technique requires only the use of a few drops of the prepared sol precursor. Thereby, TiO_2 thin film thickness is expected to be higher than that prepared by sol-gel spin-coating technique.

The Energy Dispersive X-ray Spectroscopy (EDS) analysis reveals the presence of the Ti, O, Ce, and Eu peaks (Figure 2). During the doping process, Ce and Eu substitute Ti in the TiO lattice which is confirmed by the increase in Ce/ Ti atomic ratio in Ce-TiO_2 thin films from 0 to up to 2.2 as the Ce amount in the precursor solution increased from 0 to 5wt% (Figure 2). Likewise, Eu/Ti atomic ratio increased from 0 to 0.35 as the Eu amount increased from 0 up to 1wt% (Figure 2).

3.2. XRD analysis

The XRD patterns of the deposited pure- TiO_2, Ce-doped TiO_2, and Eu-doped TiO_2 thin films elaborated by dip coating and annealed at 500 °C, are illustrated in Figure 3. The obtained X-rays diffraction patterns exhibited mainly the anatase phase (JCPDS No. 21-1272) [48]. All the films showed the anatase predominant peaks having (101), (200) and (201) as orientations, and were observed, respectively at $2\theta = 25°$, $2\theta = 48°$ and $2\theta = 56°$ (Figure 3). Furthermore, the XRD patterns (Figure 3) show also another dominant peak at $2\theta = 68°$, which corresponds to p-Si substrate [47,49]. XRD patterns showed also a rutile peak having (111) orientation and observed at $2\theta = 41°$ [50]. The calculated parameters of (101) crystal plane of the first anatase diffraction peak estimated from the Debye–Scherrer equation [51] of pure and Ce-TiO_2 thin films are defined and reported in Table 2.

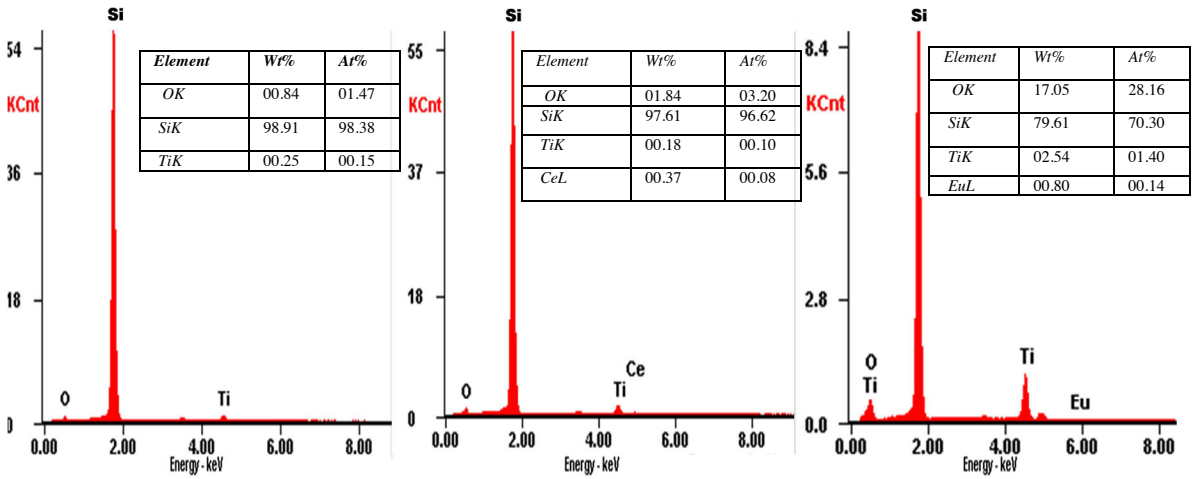

Figure 2. EDS spectra of (a) Pure-TiO_2 thin films (b) Ce-doped TiO_2 thin films (1wt%),(c) Eu- doped TiO_2 thin films (0.1wt%).

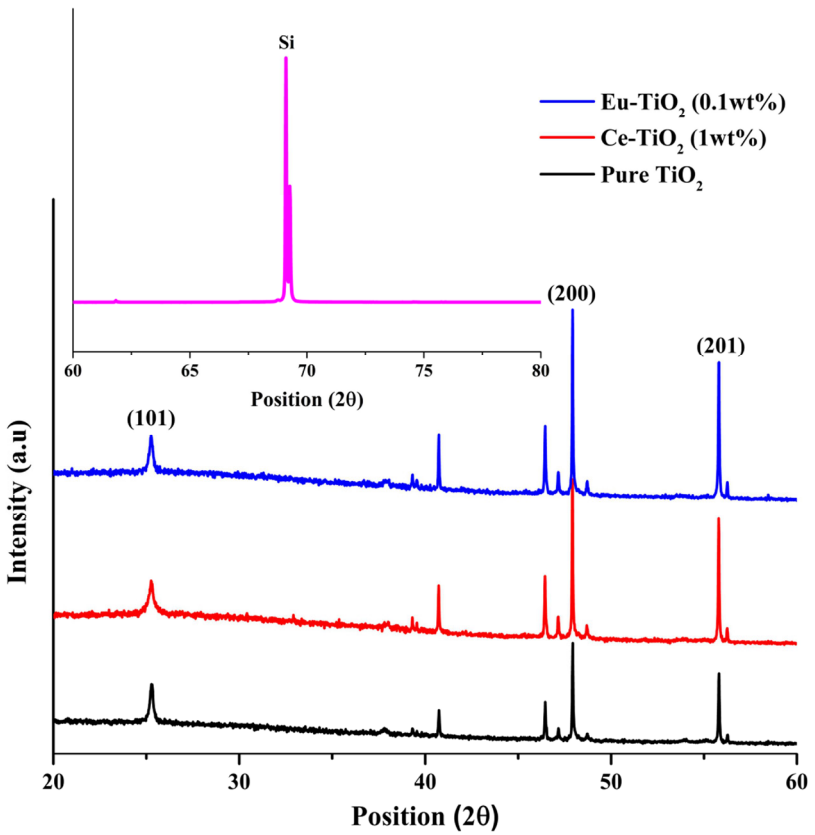

Figure 3. XRD patterns of Pure-TiO_2, Ce- doped TiO_2 (1wt%) and Eu- doped TiO_2(0.1wt%) thin films annealed at 500 °C. Inset figure (silicon substrate), A=anatase, R=rutile.

The crystallite size of TiO_2 did not change when low doping amounts were introduced. The crystalline sizes are 27.70 nm and 27.69nm, respectively for Ce-TiO_2 (1wt%) and Eu-TiO_2 (0.1wt%) compared to 27.71 nm for pure TiO_2. This behavior is confirmed by the stable anatase peak intensity after doping with Ce (1wt%) and Eu(0.1wt%), which revealed that the crystallinity of TiO_2 lattice was not damaged after doping at a low amount (Figure 3). However, on Ce doping at a high amount, the anatase grain growth is hindered and the crystallite size decreased to 20.88 nm. This result is in

agreement with the literature [52], Ce ions doped into host lattice leads to the creation of imperfection in the crystal structure. The crystal lattice expansion reduces the growth of anatase and thereby, the crystallite size was decreased [53].

3.3. Raman analysis

Figure 4 illustrates the Raman patterns of pure-TiO_2, Ce-TiO_2 (1wt%), and Eu-TiO_2 (0.1wt%) thin films annealed at 500 °C for 2 h. It can be observed that there are five characteristics of active bands for the Raman spectrum of anatase which are (A_{1g} + 2B_{1g} + 3E_g). Hence, Raman bands appeared at 146 (E_g), 197 (E_g), 397 (B_{1g}), 522 (B_{1g}), and 640 (E_g) cm^{-1} are very distinctive and can be assigned to anatase phase, for all deposited thin films (Figure 4). Accordingly, it has been reported that in the Raman spectrum of anatase single crystal, the allowed modes appeared at 144 (E_g), 197 (E_g), 399 (B_{1g}), 516 (A_{1g}), 519 (B_{1g}), and 639 cm^{-1} (E_g) [54,55]. This finding is in accordance with XRD spectra analysis (Figure 3). In fact, Eg peak appears due to O–Ti–O symmetric stretching vibration in TiO_2, B_{1g} peak appears due to O–Ti–O symmetric bending vibration and A_{1g} peak appears due to O–Ti–O antisymmetric bending vibration [55,56]. Raman spectra showed also

Table 2. Effect of different Ce and Eu content on calculated parameters of (101) crystal plane of the first anatase peak diffraction at 500 °C during 2h for Pure- TiO_2, Ce-doped TiO_2 and Eu-doped TiO_2 thin films.

Sample	Position (2Θ)	FWHM	d- spacing (nm)	Average cristalline size D (nm)
Pure TiO_2	25.30	0.307	3.03	27.71
Ce-TiO_2 (0.1 wt%)	25.24	0.307	3.03	27.69
Ce-TiO_2 (0.5 wt%)	25.28	0.307	3.04	27.70
Ce-TiO_2 (1 wt%)	25.28	0.307	3.03	27.70
Ce-TiO_2 (3 wt%)	25.22	0.307	3.53	27.69
Ce-TiO_2 (5 wt%)	25.20	0.409	3.53	20.88
Eu-TiO_2 (0.1 wt%)	25.25	0.307	3.03	27.69
Eu-TiO_2 (0.5 wt%)	25.27	0.307	3.03	27.69
Eu-TiO_2 (1 wt%)	25.25	0.307	3.03	27.69

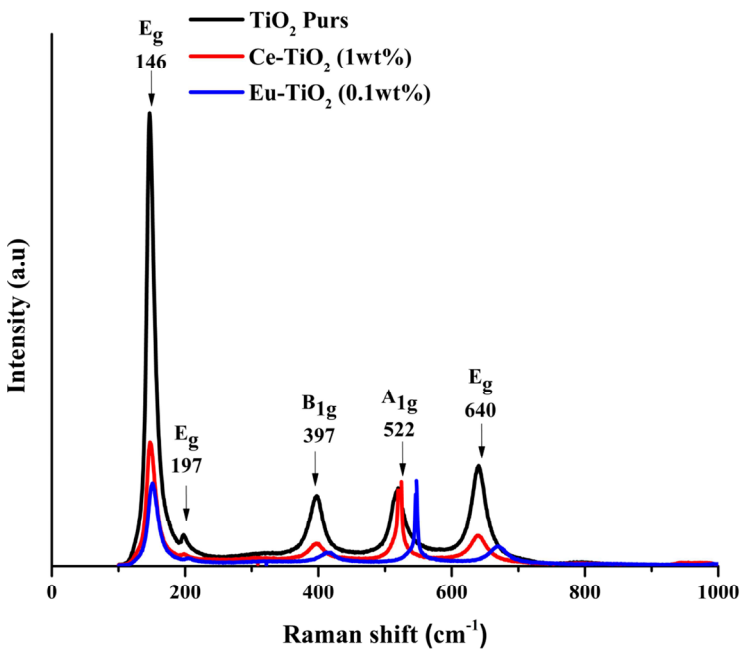

Figure 4. Raman spectra of pure- TiO_2, Ce-doped TiO_2 (1wt%), and Eu-doped TiO_2 (0.1wt%) thin films annealed at 500 °C for 2h.

distinct trends in the peak position of E_g mode with Ce and Eu doping to higher wavenumbers, respectively from 146cm^{-1} to 152cm^{-1} for 5wt% Ce-TiO_2 and to 147cm^{-1} for 1wt% Eu-TiO_2. The ionic size of Ce^{3+}(0.111 nm), Ce^{4+}(0.101 nm), Eu^{3+} (0.095 nm), and Eu^{2+} (0.109 nm) are larger than Ti^{4+}(0.068 nm) ionic size, hence, doping TiO_2 with Ce and Eu ions will distort the lattice structure of TiO_2 and generates oxygen vacancies [56]. Oxygen vacancies generated are responsible for the shifting of the first Eg Raman peak [7]. Besides, the diminishing of Eg intensity after doping may be due to the breakdown of long-range translational crystal symmetry caused by the incorporated defects of Ce and Eu dopant ions [57].

3.4. Photo-electrochemical characterization

3.4.1. Photopotential measurements

The response of photopotential measurements (Eocp) in an alkaline medium (NaOH 0.1M) during on/off cycle of UV irradiation is illustrated in Figure 5. During UV irradiation, the open circuit potential shifted towards more negative values for pure TiO_2, Ce-TiO_2 (1wt%), and Eu-TiO_2 (0.1wt%) electrodes. The more cathodic values of Eocp indicated that more electrons were generated in the conduction band of the Ce-TiO_2 (1wt%) and Eu-TiO_2 (0.1wt%) photocatalysts, thus, the photogenerated charge carriers were successfully separated [34]. On the contrary, an exponential behavior appeared by cutting UV irradiation. The slow relaxation indicated a long lifetime of the electrons and holes for the Ce-TiO_2 (1wt%) and Eu-TiO_2 (0.1wt%) compared to pure TiO_2 photocatalyst and an expected better photocatalytic activity during photodegradation reaction.

3.4.2. EIS measurements p-Si and TiO_2/ p-Si diagrams

In the dark before UV illumination, the Nyquist diagram of p-Si substrate (Figure 6a) presented two responses at high and low frequency ranges. It started by a semicircle at the high frequency range, then an almost vertical line of the curve, presenting a highly capacitive behavior (Figure 6a) characteristic of the semiconductor oxides. The same behavior is observed when the TiO_2 film is fixed on the Si substrate. However, the high frequency loop presented a lower resistance and the highly capacitive behavior is attenuated (Figure 6b). This EIS behavior in the dark was represented by a circuit in the low frequency range (R_T-C_{PE}), that describes the behavior of the space charge layer of the semiconducting oxide (Figure 7a), where C_{PE} is used instead of pure capacitance. On the other hand, the second ($R_{SS}C_{SS}W_{SS}$) circuit in the high frequency range describes the relaxation of charges via surface states (Figure 7a), where R_{SS}, $C_{SS,}$ and W_{SS} are respectively associated with the resistance, capacitance of surface states and Warburg element used to obtain a better fit. Both components of the equivalent circuit models are connected in parallel and the resulting circuit is connected in series with the electrolyte resistance (Rs) (Figure 7a). This proposed model was applied in previous work [58,34,59]. Table 3 presents the electrical components of the equivalent circuits before and after UV irradiation after fitting the experimental data of EIS diagrams using the software ZSimpWin3.2 with fitting error between E-3 and E-4. It was confirmed that the highly capacitive

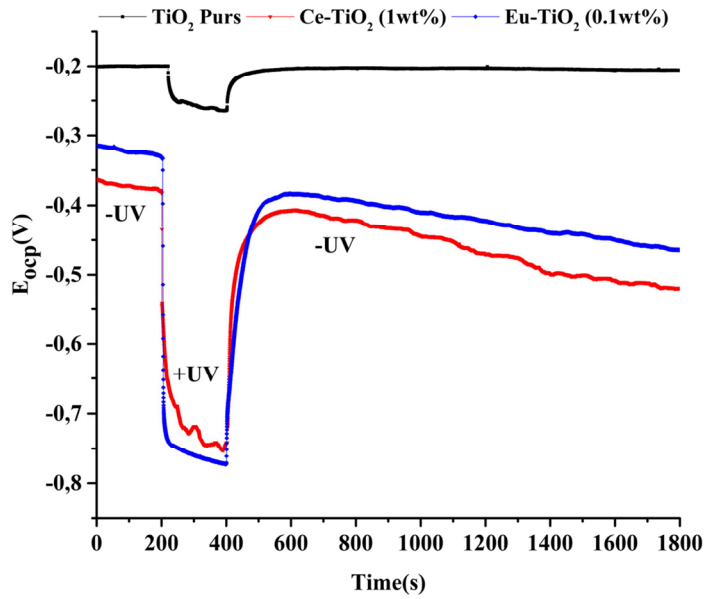

Figure 5. Open-circuit photopotential of Pure TiO_2, Ce-TiO_2 (1wt%), and Eu-TiO_2 (0.1wt%) electrodes during UV On/Off cycle.

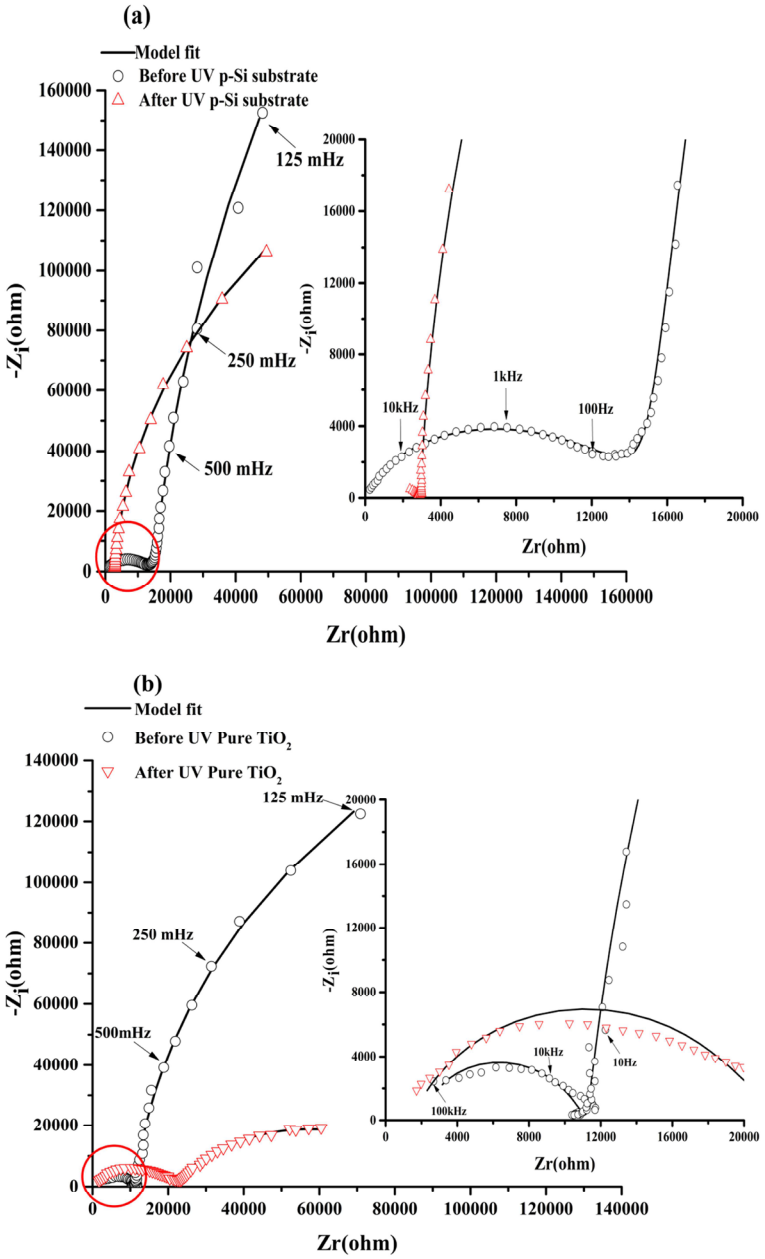

Figure 6. EIS in Nyquist representation (a) for p-Si and (b) Pure TiO_2 electrodes in the dark before UV irradiation and after 2h of UV irradiation registered at open circuit potential in NaOH (0.1M).

behavior (n = 0.95) decreased slightly after fixation of the TiO_2 film (n = 0.94), however, the R_T decreased strongly from 1.17E6 to 4.036E5 (Ω) as observed by comparing the two Figures (6a and 6b). The presence of TiO_2 at the p-Si surface decreased the space charge layer of the electrode. In the case of UV illumination for 2h and back to the dark for 1h, a set of new impedance diagrams was performed to evaluate the long-lasting photo-induced changes in the synthesized thin films. The experimental EIS plot of p-Si and TiO_2 film on p-Si, showed the two time constant loops at the high and low frequencies. However, the arc radius at low frequency decreased in the two cases (Figures 6a and 6b), indicating that two electrodes possessed a lower electron transfer resistance after UV irradiation which leads to a faster interfacial charge transfer, thereby an effective separation of photogenerated electron/hole pairs occurred. Taking into accounts this charge transfer corresponding to the transfer of photogenerated holes to species in solution or present at the surface of the TiO_2

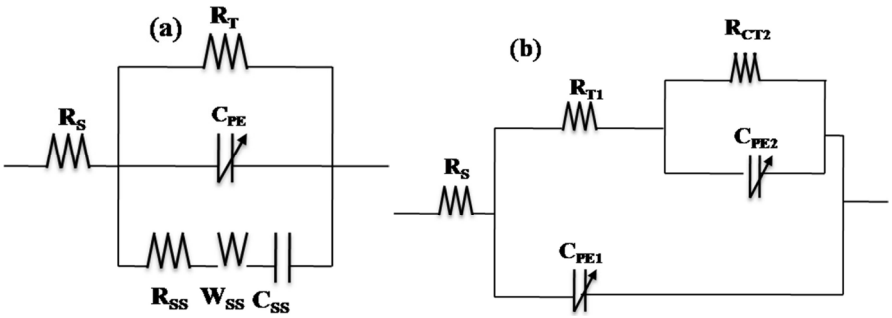

Figure 7. Equivalent circuit in the dark (a) before UV (b) after UV illumination.

Table 3. Numerical results for the electrical components used in the equivalent circuits.

Before UV illumination	$R_S(\Omega)$	$R_T(\Omega)$	$C_{PE}(\Omega^{-1}s^n)$	**n**	$R_{SS}(\Omega)$	$C_{SS}(\mu F)$	$W_{SS}(\mu F)$
p-Si	1.74E2	1.17E6	7.82E-6	9.5E-1	1.55E4	2.25E-9	7.7E-7
PureTiO_2	2.21E3	4.036E5	8.01E-6	9.4E-1	9.28E3	5.26E-10	8.92E-8
Ce-TiO_2 (1wt%)	57.92	8.26E4	1.28E-6	8.8E-1	4.29E4	1.08E-8	1.58^E-6
Eu-TiO_2 (0.1wt%)	2.63E2	8.01E4	1E-5	7.8E-1	1.29E4	9.66E-9	2.41E-6
After UV illumination	$R_S(\Omega)$	$R_{T1}(\Omega)$	$C_{PE1}(\Omega^{-1}s^n)$	n_1	$R_{CT2}(\Omega)$	$C_{PE2}(\Omega^{-1}s^n)$	n_2
p-Si	1.47E3	2.83E3	1.77E-8	6.4E-1	2.8E5	9.57E-6	9.74E-1
Pure TiO_2	1.47E3	1.92E4	1.18E-8	8E-1	7.34E4	1.428E-5	6E-1
Ce-TiO_2 (1wt%)	1.86E2	7E3	8.71E-7	6.2E-1	1.6E4	1.04E-3	9.9E-1
Eu-TiO_2 (0.1wt%)	27E2	3E3	1.94E-7	8E-1	1E4	1.21E-4	4.7E-1

semiconductor, the corresponding equivalent circuit model proposed can be described using two R_T-C_{PE} circuits (Figure 7b). The small semicircle at high frequency range corresponds to the resistance for the charge transfer from p-Si through TiO_2 to the surface (R_{T1}, C_{PE1}), whereas the large semicircle at low frequency range corresponds to the photoelectrode/electrolyte interfacial charge transfer resistance (R_{CT2}, C_{PE2}). Similar models have been adopted by other work [60]. The parameters of the equivalent circuit are summarized in the same Table 3.

Doped Ce or Eu-TiO_2/p-Si diagrams Ce-TiO_2/p-Si electrode

In the dark before UV illumination, the Nyquist diagrams of Ce-TiO_2 (Figure 8a) did not present separation of the two observed loops. The related time constants seem to be in the same range or the time constant of the high frequency loop increased strongly from $\tau=210^{-3}$ms for non doped TiO_2 to τ = 1.27ms due to the doping. The low frequency limit is near to 80000 (Ω) (Figure 8a) very low compared to the non doped electrode (Figure 6b). The Ce doping improved strongly the charge transfer in the dark. The R_T decreased to 8.26E4 (Ω) compared to the non doped electrode (4.036E5)(Ω) (Table 3). In the dark after UV illumination, the interface has the same behavior but the limit of the low frequency decrease drastically near to 16000(Ω) indicating that after UV irradiation the Ce-TiO_2 electrode possessed a lower electron transfer resistance which leads to a faster interfacial charge transfer, which can lead to effective separation of photogenerated electron/hole (Figure 8a). Besides, the charge transfer resistance R_{CT2} decreased from 8.26E4 to 1.6E4(Ω) in comparison with the non doped electrode 7.34E4 (Ω) after UV illumination.

Eu-TiO_2/ p-Si electrode

In the dark before UV illumination, the Nyquist diagrams of Eu-TiO_2 (0.1wt%) showed a similar behavior compared to the non doped electrode with two separated loops but without a strong capacitive component (Figure 8b). The arc radius is lower, suggesting also an improved charge transfer due to the Eu doping. After UV illumination, the decrease is stronger and the Eu- doped electrode presented the lowest electron transfer resistance. In fact, the charge transfer resistance R_{CT2} decreased from 8.01E4 to 1E4 (Ω) compared to the non doped electrode (7.34E4 Ω after UV illumination). High carrier flow from the electrode to the interface with the solution is expected to lead to high separation between the photogenerated holes and electron and potentially high efficiency of the photocatalytic process when using this newly developed photocatalyst.

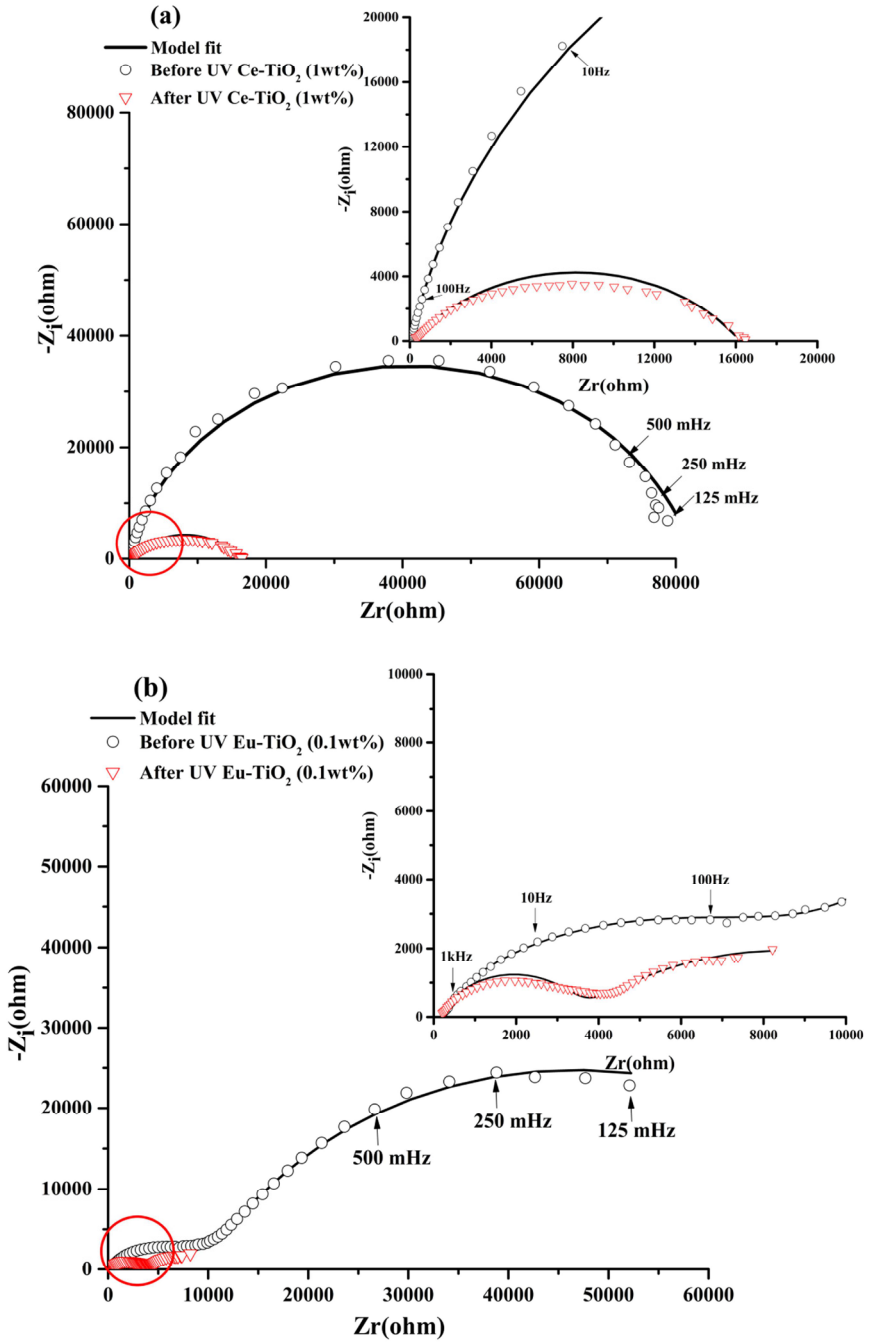

Figure 8. EIS in Nyquist representation for (a) Ce-TiO_2 (1wt%) and (b) Eu-TiO_2(0.1wt%) electrodes in the dark before UV irradiation and in the dark after 2h of UV irradiation registered at open circuit potential in NaOH (0.1M).

3.5. Photodegradation experiments

The photocatalytic activity of pure Ce-TiO_2 and Eu-doped TiO_2 thin films was tested by investigating the photodegradation of AB under UV illumination. The obtained photodegradation efficiencies of AB (C_0 = 10ppm, pH = 3.5) within 30 min, were summarized in Figure 9a. As shown in Figure 9a, doping TiO_2 thin films by Eu ions increased the photodegradation efficiency after 30 min from 35.2% to 60%-66.4% depending on Eu amount (0.1, 0.5, and 1wt%). However, on Ce-doping, the photodegradation efficiency was enhanced from 35.2% to 50% after 30 min at optimal Ce amount (1wt%). Therefore, the best performance in AB removal was observed in the presence of Eu-ions dopant at an optimal concentration of

0.1wt%. Besides, the efficiencies were about 98.94%, 98.21%, and 97.13%, respectively for (Eu: 0.1, 0.5, and 1wt%) after 120 min of reaction time. It is worth noting that, the AB removal by photolysis reaction was about 60.52% after 120 min of reaction, which confirms the enhancement role of the developed photocatalysts, pure and Ce and Eu-TiO_2 thin films. The UV-Vis spectra of AB are characterized by a remarkable peak at 620 nm and two ultraviolet peaks at 226 and 318 nm (Figure 9b). The peak at 620 nm is related to the presence of the azo chromophore group (N=N) (Figure 9b) [59]. While the peaks observed at 226 and 318nm (Figure 9b) are related respectively to the aromatic benzene and naphthalene groups [62,63]. After 120 min of photodegradation by pure TiO_2 thin films, the aqueous solution of AB became totally colorless. The disappearance of the peaks at 226 nm and 318 nm (Figure 9b), indicates the degradation of AB under the experimental conditions (pH = 3.5, C_0 = 10ppm). However, the intense peak at 620 nm decreased faster (35.19%) than the ultraviolet peak at 318 nm (24.28%) after 30 min (Figure 9b). It means that during the degradation mechanism, •OH radicals attack preferentially –N = N– group than the benzene and naphthalene groups and confirms the results of other works related to azo dyes [64]. The linear fit under optimal conditions of pH = 3.5 and C_0 = 10 ppm can be approximated as apparent-first-order kinetics reaction. The apparent first-order kinetics of AB photodegradation are illustrated in Figures (10b and 11b) according to Eq.1.

$$ln\,{}^{C}/_{C_0} = -kapp \times t \quad \text{(Eq.1)}$$

where, t and k_{app} are respectively the photodegradation time (min) and the apparent rate constant (min^{-1}).

The parameters k_{app} (min^{-1}) and R^2 (correlation coefficient) are mentioned in Figures (10b and 11b). After Ce-doping, k_{app} of AB photodegradation slightly increased from k_{app} = 0.022 min^{-1} for pure TiO_2 to k_{app} = 0.026 min^{-1} at optimal Ce amount (1wt%) corresponding to 96.44% of AB removal. But, it greatly increased from k_{app}=0.022 min^{-1} for pure TiO_2 to k_{app} = 0.036 min^{-1} at optimal Eu amount (0.1wt%) reaching 98.94% of AB removal. Besides, the removal of AB was faster using Eu-doped TiO_2 photocatalysts ($t_{1/2}$ = 2min) than that of pure TiO_2 ($t_{1/2}$ = 45 min) and Ce-TiO_2 (1wt%) ($t_{1/2}$ = 30 min). However, it was clearly shown in Figures 10 and 11 that increasing the amount of Ce and Eu ions above an optimal amount (1wt% Ce) and (0.1wt% Eu), led to the decrease in k_{app} to k_{app} = 0.030 min^{-1} and k_{app} = 0.014 min^{-1}, respectively at Eu (1wt%) and Ce (5wt%). These results could be due to the presence of surface oxygen vacancies and Ti^{3+} surface states on the pure TiO_2 surface that are not high enough to trap all the exciting photogenerated electron/hole pairs. Thereby, fewer amount of electrons and holes pairs are available to interact with the AB molecule [52]. Thus, adding appropriate amount of Ce and Eu ions led to better electron scavenging capacity due to the ability of unoccupied 4f orbital of Ce and Eu ions to accept electrons [65,66]. As a matter of fact, the electrons trapped in $Ce^{4+}/Ce^{3+}$and Eu^{3+}/Eu^{2+} sites were subsequently transferred to the adsorbed O_2 and produced superoxide radicals according to Equations (2, 3, 4, 5, and 6) and regenerate the dopants. Finally, oxygen radicals react with the protons in the aqueous solution to produce hydroxyl radicals (•OH) according to Eq. (7). Consequently, the photogenerated electron was transferred efficiently [8,67].

$$TiO_2 + h\nu \rightarrow e^- + h^+ \quad \text{(Eq.2)}$$

$$Ce^{4+} + e^- \rightarrow Ce^{3+} \quad \text{(Eq.3)}$$

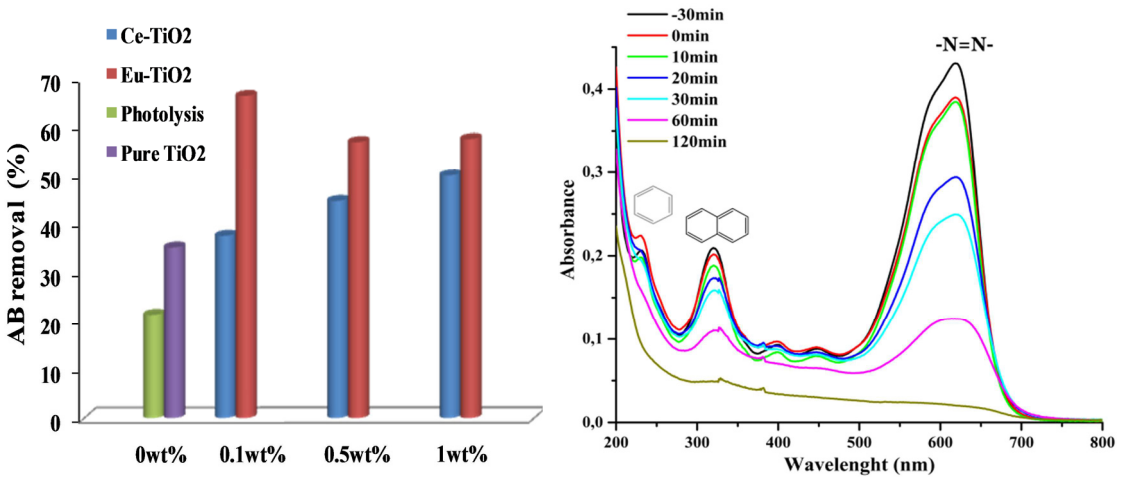

Figure 9. (a) AB removal (%) after 30 min of photodegradation by of Ce and Eu-TiO_2 thin films (b) UV-Vis spectra of amido black withdrawn at different interval times for pure TiO_2.

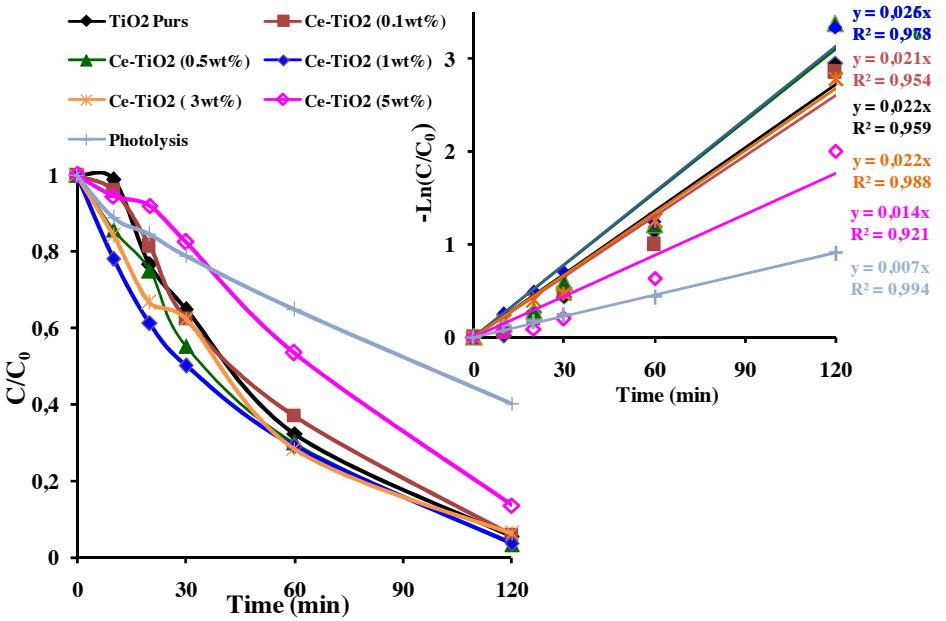

Figure 10. (a) C/C_0 plot (b) Apparent 1st order kinetics plot of AB (C_0 = 10 ppm; pH= 3.5; λ = 620nm) for Ce-TiO_2 thin films.

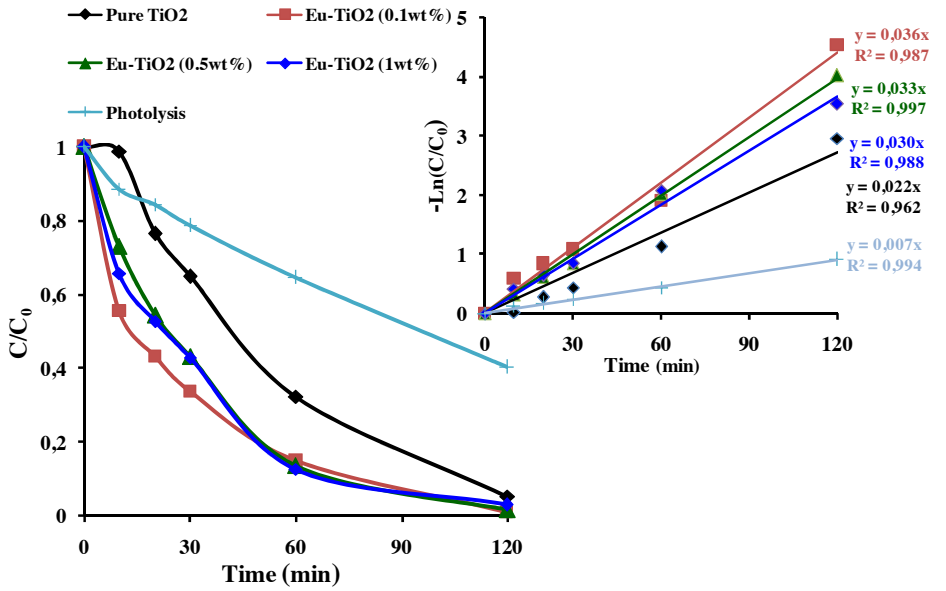

Figure 11. (a) C/ C_0 plot (b) Apparent 1st order kinetics plot of AB (C_0 = 10ppm; pH=3.5; λ = 620nm) for Eu-TiO_2 thin films.

$$Ce^{3+} + O_2 \rightarrow Ce^{4+} + O_2^{\bullet -} \quad \text{(Eq.4)}$$

$$Eu^{3+} + e^- \rightarrow Eu^{2+} \quad \text{(Eq. 5)}$$

$$Eu^{2+} + O_2 \rightarrow Eu^{3+} + O_2^{\bullet -} \quad \text{(Eq. 6)}$$

$$O_2^- + 2H^+ \rightarrow 2OH^{\bullet -} \quad \text{(Eq.7)}$$

However, according to Figures 10 and 11, the decrease in the photodegradation efficiency and k_{app} when Ce and Eu amounts exceed respectively, 1wt% and 0.1wt% could be due to the reduction of the active sites on TiO_2 surface covered by the excess amount of Ce and Eu ions [11]. On the other hand, when Ce and Eu dopant ions exceeded an optimal

concentration, the thickness of the space charge layer (W) narrowed compared to the penetration depth of UV light. Thereby, increasing the recombination rate of electron/ hole pairs [52]. In summary, according to the present results, it was found that doping TiO_2 thin films with Eu dopant ions greatly increase the photodegradation efficiency of AB than Ce dopant ions. The best photocatalyst (Eu-TiO_2 0.1wt%) will be considered in the following of this study for an optimization of the photocatalytic process.

3.5.1. Effect of pH

To study of the effect of pH in aqueous medium, the photocatalysts presenting the best photocatalytic activity Eu-TiO_2 (0.1wt%) was considered. The photodegradation efficiencies of AB were studied at an initial pH range between 3.5 and 9 and C_0 = 10ppm. It was found that the initial pH greatly affected the AB removal since it decreased from 98.94% to 66.90% (Figure 12), respectively when pH increased from 3.5 to 9. The parameters k_{app} and R^2 are mentioned in Figure 12 and Table 4. A decrease in k_{app} of AB photodegradation was shown from k_{app}=0.036 min^{-1} to k_{app}=0.009 min^{-1}, respectively for pH (3.5) to pH (9) (Table 4). As the TiO_2 has an amphoteric behavior; the variation of pH solution changes its surface charge and shifts the catalytic reactions potentials [68,69]. In fact, the surface of TiO_2 photocatalyst can be protonated in acidic media (Eq.8) or deprotonated in alkaline media (Eq.9).

$$TiOH + H^+ \rightarrow TiOH_2^+ \; pH < pzc \quad \text{(Eq.8)}$$

$$TiOH + OH^- \rightarrow TiO^- + H_2O \; pH > pzc \; [70] \quad \text{(Eq.9)}$$

TiO_2 has a pHpzc value of 6.25 which causes TiO_2 to be positively charged at pH below pHpzc and to be negatively charged at pH above pHpzc. The lack of information about the pKa of AB dye, makes the prediction of its structure (protonated or ionic), which depends on the pH of the solution, more complex [71]. However, according to the present results, the optimum pH obtained is in the acidic range pH (3.5), where the Eu-TiO_2 (0.1wt%) photocatalyst is positively charged, leading to the prediction of the AB molecule to be negatively charged. Thus, resulting in a favorable attraction between the Eu-TiO_2 (0.1wt%) surface and the AB dye in the acidic solution and columbic repulsion in the alkaline solution [69,72]. Moreover, at lower pH, holes act as major oxidation species and at neutral or high pH, hydroxyl radicals are considered as the major oxidation species [73]. Therefore, under alkaline conditions the presence of hydroxyl ions may neutralize the acidic end-products produced by the photodegradation reaction, thus leading to a decrease in the photodegradation of amido black [74]. As a consequence, the photodegradation efficiency of AB under acidic medium is enhanced by the positive holes which are considered as the major oxidation species at low pH and the strong adsorption of the anionic dye molecules on the positive surface of the photocatalyst [75].

3.5.2. Effect of dye concentration

The initial dye concentration is an important factor that affects the photocatalytic degradation of AB. The effect of initial dye concentration was studied by varying the initial concentration to (C_0 = 10,20,30 and 40 ppm) at constant pH = 3.5 under optimal conditions of atomic weight percentage of Eu (0.1wt%). According to Figure 13, the reaction rates of AB

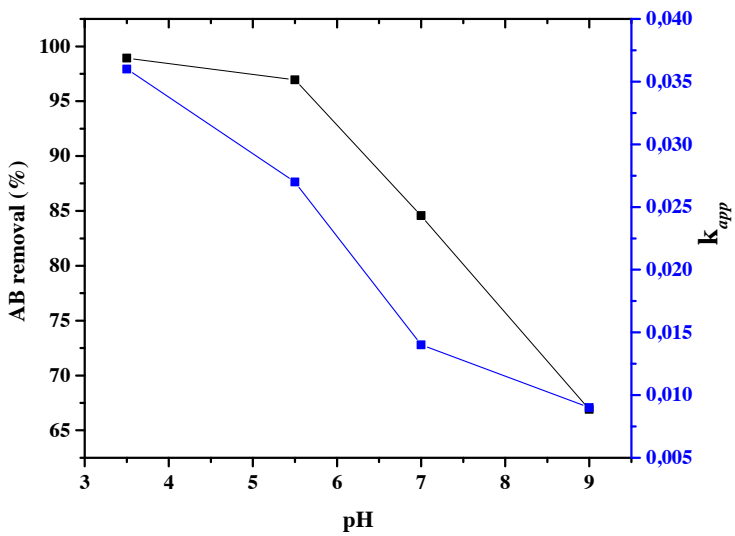

Figure 12. AB removal (%) and k_{app} (min^{-1}) for Eu-TiO_2 (0.1wt%) thin films at C_0 = 10 ppm; λ = 620 nm and different pH.

Table 4. Kinetic parameters of AB photodegradation by Ce and Eu-TiO_2 under different pH and AB concentration.

Photocatalyst	pH	C_0 ppm	k_{app} (min^{-1})	R^2	pH	C_0 ppm	k_{app} (min^{-1})	R^2
Eu-TiO_2 (0.1wt%)	3.5 5.5 7.0 9	10	0.036 0.027 0.014 0.009	0.987 0.983 0.980 0.968	3.5	10 20 30 40	0.036 0.019 0.008 0.005	0.987 0.982 0.974 0.996
Ce-TiO_2 (1wt%)	3.5	10	0.026	0.978				
Pure TiO_2	3.5	10	0.022	0.959				
Photolysis	3.5	10	0.007	0.994				

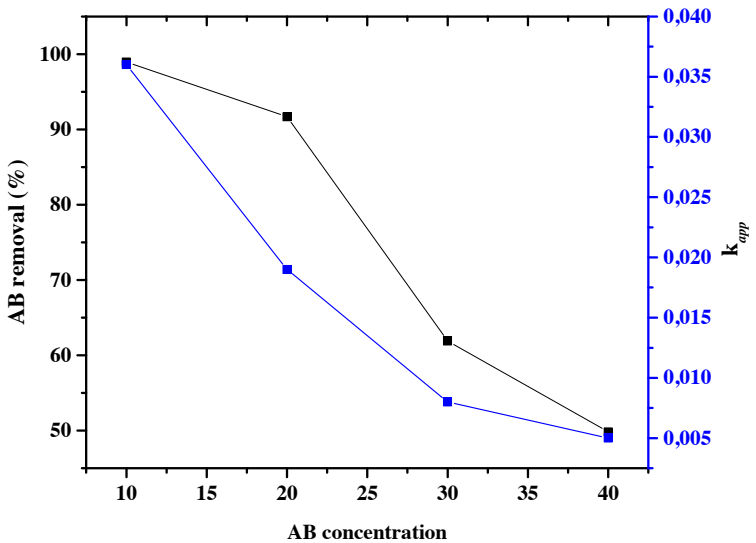

Figure 13. AB removal (%) and k_{app} (min^{-1}) for Eu-TiO_2 (0.1wt%) thin films at pH = 3.5; λ = 620 nm and different AB concentrations.

photodegradation decrease from k_{app} = 0.036 min^{-1} for C_0 = 10ppm to k_{app} = 0.005 min^{-1} for C_0 = 40ppm in accordance with the decrease in the photodegradation efficiency (Table 4). In fact, the photodegradation efficiency of AB decreased from 98.94% to 49.85%, respectively when C_0 increased from 10 ppm to 40 ppm. Similar results have been reported for the photodegradation of AB dye [63]. The more the initial dye concentration increases, the more organic substances are adsorbed on the surface of TiO_2, whereas less number of photons are available to reach the catalyst surface, and therefore less •OH are formed, thus resulting in the decrease of the degradation efficiency. The penetration of light to the surface of the catalyst is the limiting step [69,74]. On another side, the high coloration of the solution due to the high concentration of the colorant prevents the catalyst from being excited and favorites the photolysis of AB.

3.5.3. Degradation pathways and oxidation reaction intermediates of AB

The photodegradation of AB by Eu-TiO_2 (0.1wt%) thin films, under optimal conditions (pH = 3.5, C_0 = 10ppm), was investigated using HPLC and compared to pure TiO_2 photocatalyst. The chromatograph shows that the intense peak at the retention time of 2.53 min refers to the AB dye molecule. After decolorization occurred, the chromatogram of the degraded dye showed a considerable decrease of the major peak (Figure 14). The disappearance of the AB dye peak was followed by a generation of new peaks at 2.25 min and 1.97 min retention time, in the HPLC chromatogram of AB photodegradation reaction (Figure 14). Thus, we can confirm the degradation of the initial AB dye molecule and its transformation into intermediates. Based on the mechanisms of amido black degradation proposed by [63], it was reported that the degradation of AB is initiated by radical attack on preferential sites of the molecules, the nitro, sulfonate, and azo groups. The degradation pathway can be complex and can lead to the generation of a multitude of intermediates. 4-amino-6-diazenyl-5-hydroxy-3-((4-nitrophenyl)diazenyl)naphthalene-2,7-disulfonate (G1) is considered as a major intermediate

[63]. Then the attack of •OH radicals produced sodium 3,4,6-triamino-5-hydroxynaphthalene-2,7-disulfonate (G2) (Figure 14). According to current investigation, the apparition of two intermediates peaks at 1.97 min and 2.25 min, respectively after 10 min and 30 min of starting the photodegradation reaction, could be correlated to the fragment (G1) and (G2) detected by [63] after photodegradation of amido black 10B by Polycarbazole-Decorated TiO_2 Nanohybrids (Figure 14). Furthermore, the apparent-first constant of AB degradation using Eu-TiO_2 (0.1wt%) photocatalyst under 60 min of photodegradation reaction was about k_{app} = 0.041min^{-1} compared to k_{app} = 0.032min^{-1} for pure TiO_2 (Figure 15). This confirms that doping TiO_2 thin films with Eu ions with an appropriate amount (0.1wt%) leads to an enhancement of mineralization efficiency of AB dye obtained by HPLC results, which is in accordance with UV-Vis results that showed an enhancement of AB discoloration by the Eu-TiO_2(0.1wt%) photocatalyst. In summary, the degradation mechanism can be assumed to be the •OH radicals attack of the azo groups of AB molecule [76].

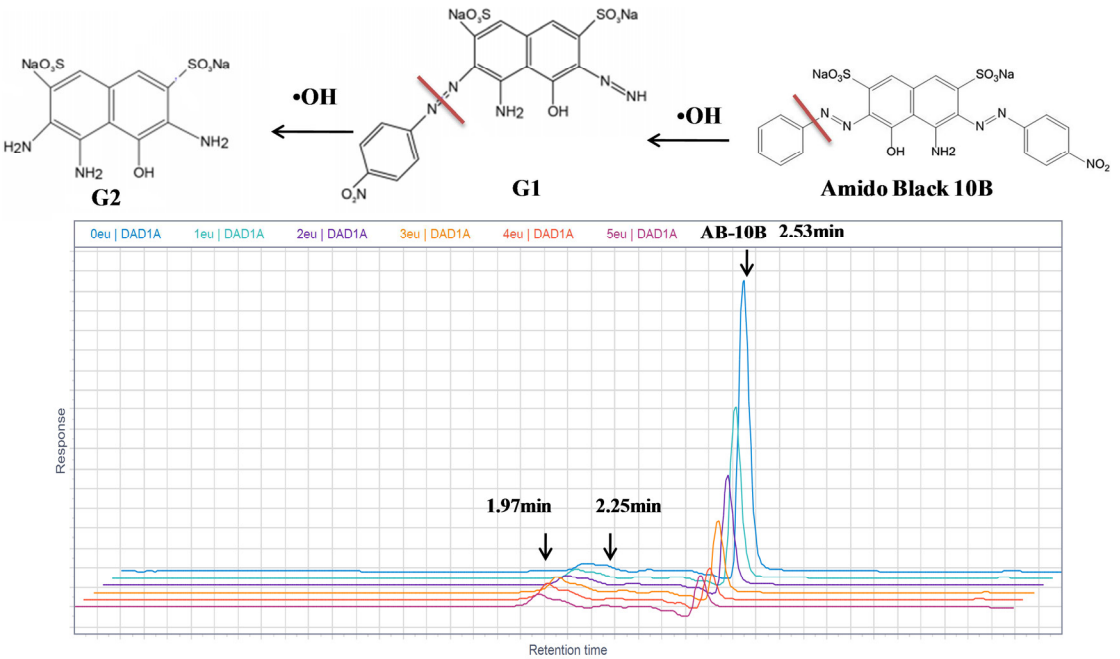

Figure 14. Proposed amido black 10B degradation pathway [61] and high-performance liquid chromatograms of AB obtained at different interval times of irradiation (pH = 3.5, C_0 = 10 ppm), using Eu (0.1wt %) doped TiO_2 films.

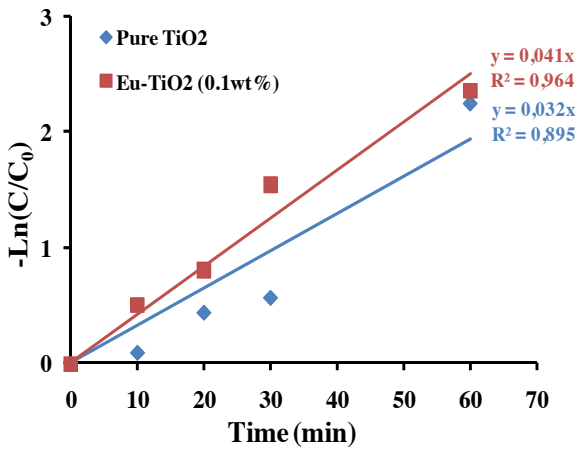

Figure 15. Photocatalytic mineralization of AB in aqueous solution (C_0 = 10ppm, pH = 3.5) using Pure TiO_2 and Eu-TiO_2 (0.1wt%) photocatalyst.

4. Conclusion

In summary, Ce and Eu-TiO_2 thin films were synthesized successfully by sol-gel dip-coating technique and coated on silicon wafers by a sol precursor solution containing different ratio of Ce and Eu ions. EIS measurements revealed that the doped TiO_2 photocatalyst by Ce and Eu ions presented a faster interfacial charge transfer and an expected higher photocatalytic activity during the photoreaction, which was confirmed by the photodegradation results. According to the present study, doping TiO_2 thin films with Eu ions can effectively enhance the photodegradation and the mineralization efficiency of AB removal at an optimal concentration of Eu (0.1wt%) for better electron/hole pairs separation. The reaction rate constant k_{app} of AB removal by Eu-TiO_2 (0.1wt%) was about k_{app} = 0.036 min^{-1} and $t_{1/2}$ was around 12 min compared to ($t_{1/2}$ = 45 min, $t_{1/2}$ = 30 min) and (k_{app} = 0.022 min^{-1}, k_{app} = 0.026 min^{-1}), respectively for Pure TiO_2 and Ce-TiO_2 (1wt%) photocatalysts.

The study also revealed that the initial pH and AB concentration greatly affected the photodegradation of AB. The maximum photodegradation efficiency reached 98.94% in acidic media at pH = 3.5 and C_0 = 10ppm.

Acknowledgment and/or disclaimers, if any

The authors wish to acknowledge the facilities and support provided by the Department of Green Chemistry, Lappeenranta University of Technology, Sammonkatu 12, FI-50130 Mikkeli, Finland. This research was financially supported by the Tunisian Ministry of Higher Education and Scientific Research under an objective contract.

References

1. Li Y, Liu F, Li M, Wang X, Qi X et al. Synergetic effect between adsorption and photodegradation on rGO/TiO_2/ACF composites for dynamic toluene gaseous removal. Environmental Science and Pollution Research 2020; 27: 9866-9881. doi: 10.1007/s11356-019-07565-x
2. Nakata K, Fujishima A. TiO_2 photocatalysis: Design and applications. Journal of Photochemistry and Photobiology C 2012; 13: 169-189. doi: 10.1016/j.jphotochemrev.2012.06.001
3. Chong MN, Jin B, Chow CWK, Saint C. Recent developments in photocatalytic water treatment technology: A review. Water Research 2010; 44: 2997-3027. doi: 10.1016/j.watres.2010.02.039
4. McCullagh C, Skillen N, Adams M, Robertson PKJ. Photocatalytic reactors for environmental remediation: A review. Journal of Chemical Technologie and Biotechnology 2011; 86: 1002-1017. doi: 10.1002/jctb.2650
5. Kitazawa S, Yamamoto S, Asano M, Saitoh Y, Ishiyama S. Radiation-induced luminescence from TiO_2 by 10, 20 and 30 keV oxygen ion irradiations. Nuclear Instrument and Methods in Physics Research section B: Beam interactions with materials and atoms 2007; 256: 233-237. doi: 10.1016/j.nimb.2006.12.008
6. Ghosh S, Das AP. Modified titanium oxide (TiO_2) nanocomposites and its array of applications: a review. Toxicoogical and Environmental Chemistry 2015; 97: 491-514. doi: 10.1080/02772248.2015.1052204
7. Choudhury B, Dey M, Choudhury A. Defect generation, d - d transition and band gap reduction in Cu-doped TiO_2 nanoparticles. International Nano Letters 2013; 2-9.
8. Kong J, Wang Y, Sun Q, Meng D. Synthesis and photocatalytic properties of Ce-Doped TiO_2 nanotube arrays via anodic oxidation. Journal of Electron Materials 2017; 46: 4791-4797. doi: 10.1007/s11664-017-5418-8
9. Fan X, Wan J, Liu E, Sun L, Hu Y, Li H et al. High-efficiency photoelectrocatalytic hydrogen generation enabled by Ag deposited and Ce doped TiO_2 nanotube arrays. Ceramics International 2015; 41: 5107-5116. doi: 10.1016/j.ceramint.2014.12.083
10. Priyanka KP, Anu Tresa S, Jaseentha OP, Varghese T. Cerium doped nanotitania-extended spectral response for enhanced photocatalysis. Materials Research Express 2014; 1. doi: 10.1088/2053-1591/1/1/015003
11. Khade GV, Gavade NL, Suwarnkar MB, Dhanavade MJ, Sonawane KD et al. Enhanced photocatalytic activity of europium doped 2 under sunlight for the degradation of methyl orange. Journal of Materials Science: Materials in Electronics 2017; 28: 1-10. doi: 10.1007/s10854-017-6883-9
12. Kityakarn S, Pooarporn Y, Songsiriritthigul P, Worayingyong A, Robl S et al. (Photo)Electrochemical characterization of nanoporous TiO_2 and Ce-doped TiO_2 sol-gel film electrodes. Electrochimica Acta 2012; 83:113-124. doi: 10.1016/j.electacta.2012.07.129
13. Kumar M, Gupta AK, Kumar D. Mg-doped TiO_2 thin films deposited by low-cost technique for CO gas monitoring, Ceramics International 2016; 42: 405-410. doi: 10.1016/j.ceramint.2015.08.124
14. Manole AV, Dobromir M, Gîrtan M, Mallet R, Rusu G et al. Optical properties of Nb-doped TiO_2 thin films prepared by sol-gel method. Ceramics International 2013; 39: 4771-4776. doi: 10.1016/j.ceramint.2012.11.066

15. Lu L, Xia X, Luo JK, Shao G. Mn-doped TiO_2 thin films with significantly improved optical and electrical properties. Journal of Physics: Applied Physics 2012; 45. doi: 10.1088/0022-3727/45/48/485102

16. Wang J, Huang L. Optical properties of Fe-doped TiO_2 thin film prepared by Sol-gel. Applied Mechanics and Materials 2013; 395-396: 20-23. doi: 10.4028/www.scientific.net/AMM.395-396.20

17. Boutlala A, Bourfaa F, Mahtili M, Bouaballou A. Deposition of Co-doped TiO_2 Thin Films by sol-gel method. IOP Conference Series: Materials Science and Engineering 2016; 108: 2-7. doi: 10.1088/1757-899X/108/1/012048

18. Mondal S, Ghosh A, Piton MR, Gomes JP, Felix JF et al. A Investigation of optical and electrical properties of erbium-doped TiO_2 thin films for photodetector applications. Journal of Materials Science: Materials in Electronics 2018; 29: 19588-19600. doi: 10.1007/s10854-018-0090-1

19. Lourduraj S, Williams RV. Effect of iron doping on structural and optical properties of TiO_2 thin film by sol–gel routed spin coating technique. Journal of Advanced Dielectrics 2016; 7: 2-6. doi: 10.1142/S2010135X17500242

20. Dijkstra MFJ, Michorius A, Buwalda H, Panneman HJ, Winkelman JGM et al. Comparison of the efficiency of immobilized and suspended systems in photocatalytic degradation. Catalysis Today 2001; 66: 487-494. doi: 10.1016/S0920-5861(01)00257-7

21. Sordo C, Van Grieken R, Marugán J, Fernández-Ibáñez P. Solar photocatalytic disinfection with immobilised TiO_2 at pilot-plant scale. Water Science and Technology 2010; 61: 507-512. doi: 10.2166/wst.2010.876

22. Manassero A, Satuf ML, Alfano OM. Photocatalytic reactors with suspended and immobilized TiO_2: Comparative efficiency evaluation. Chemical Engineering Journal 2017; 326: 29-36. doi: 10.1016/j.cej.2017.05.087

23. Zhao CX, Huang Y, Wang JQ, Niu CY, Jia Y. Prediction of a new direct-gap silicon phase: T36 silicon. Physics Letters A 2019; 383: 125903. doi: 10.1016/j.physleta.2019.125903

24. Kuo TJ, Lin CN, Kuo CL, Huang MH. Growth of ultralong ZnO nanowires on silicon substrates by vapor transport and their use as recyclable photocatalysts. Chemistry of Materials 2007; 19: 5143-5147. doi: 10.1021/cm071568a

25. Zhang Y, Mandal R, Ratchford DC, Anthony R, Yeom J. Si nanocrystals/ZnO nanowires hybrid structures as immobilized photocatalysts for photodegradation. Nanomaterials 2020; 10: 1-16. doi: 10.3390/nano10030491

26. Hoa NT, Van Cuong V, Lam ND. Mechanism of the photocatalytic activity of p-Si(100)/n-ZnO nanorods heterojunction. Materials Chemistry and Physics 2018; 204: 397-402. doi: 10.1016/j.matchemphys.2017.10.070

27. Ruzgar S. The Optoelectrical properties of Li: TiO_2/p-Si photodiodes for various Li doping. Phys Status Solidi A 2020; 217: 1-11. doi: 10.1002/pssa.202000481

28. Zhou X, Xue Q, Chen H, Liu C. Currentvoltage characteristics and ethanol gas sensing properties of ZnO thin film/Si heterojunction at room temperature. Physica E: Low Dimensional Systems and Nanostructures 2010; 42: 2021-2025. doi: 10.1016/j.physe.2010.03.008

29. Bessergenev VG, Khmelinskii I V, Pereira RJF, Krisuk VV, Turgambaeva AE et al. Preparation of TiO_2 films by CVD method and its electrical, structural and optical properties. Vacuum 2002; 64: 275-279. doi: 10.1016/S0042-207X(01)00318-9

30. Alotaibi AM, Sathasivam S, Williamson BAD, Kafizas A, Sotelo-Vazquez C et al. Chemical vapor deposition of photocatalytically active pure brookite TiO_2. Thin Films Chemistry of Materials 2018; 30: 1353-1361. doi: 10.1021/acs.chemmater.7b04944

31. Hussin R, Choy KL, Hou X. Deposited TiO_2 thin films by atomic layer deposition (ALD) for optical properties. Journal of Engineering and Applied Sciences 2016; 11: 7529-7533.

32. Vilhunen SH, Sillanpää MET. Atomic layer deposited (ALD) TiO_2 and TiO_2-x-N x thin film photocatalysts in salicylic acid decomposition. Water Science and Technology 2009; 60: 2471-2475. doi: 10.2166/wst.2009.660

33. Iancu AT, Logar M, Park J, Prinz FB. Atomic layer deposition of undoped TiO_2 exhibiting p -type conductivity, ACS Applied Materials and Interfaces 2015; 7: 5134-5140. doi: 10.1021/am5072223

34. Atyaoui A, Cachet H, Sutter EMM, Bousselmi L. Effect of the anodization voltage on the dimensions and photoactivity of titania nanotubes arrays. Surface and Interface Analysis 2013; 45: 1751-1759. doi: 10.1002/sia.5317

35. Touam T, Atoui M, Hadjoub I, Chelouche A, Boudine B et al. Effects of dip-coating speed and annealing temperature on structural, morphological and optical properties of sol-gel nano-structured TiO_2 thin films. The European Ohysical Journal Applied Physics 2014; 67: 1-7. doi: 10.1051/epjap/2014140228

36. Elfanaoui A, Elhamri E, Boulkaddat L, Ihlal A, Bouabid K et al. X. Optical and structural properties of TiO_2 thin films prepared by sol e gel spin coating. International Journal of Hydrogen Energy 2010; 36: 4130-4133. doi: 10.1016/j.ijhydene.2010.07.057

37. Kumar A, Singh R, Bahuguna G. Thin Film coating through sol-gel technique thin film coating through sol-gel technique. Research Journal of Chemical Sciences 2016.

38. Panthi D, Tsutsumi A. A novel multistep dip-coating method for the fabrication of anode-supported microtubular solid oxide fuel cells. Journal of Solid State Electrochemistry 2014; 18: 1899-1905. doi: 10.1007/s10008-014-2429-8

39. Rivero PJ, Garcia JA, Quintana I, Rodriguez R. Design of nanostructured functional coatings by using wet-chemistry methods. Coatings 2018; 8. doi: 10.3390/coatings8020076

40. Abdeen DH, El Hachach M, Koc M, Atieh MA. A review on the corrosion behaviour of nanocoatings on metallic substrates. Materials 2019; 12. doi: 10.3390/ma12020210

41. Pant B, Park M, Park SJ. Recent advances in TiO_2 films prepared by sol-gel methods for photocatalytic degradation of organic pollutants and antibacterial activities. Coatings 2019; 9. doi: 10.3390/coatings9100613

42. Francesca S, Teresa FM, Teresa P, Nicolas G. Mesoporous TiO_2 Thin Films: State of the Art Chapter. In: Intech, 1989, pp. 137-144.

43. Chaki SH, Mahato KS, Malek TJ, Deshpande MP. $CuAlS_2$ thin films – Dip coating deposition and characterization. Journal of Science: Advanced Materials and Devices 2017; 2: 215-224. doi: 10.1016/j.jsamd.2017.04.002

44. Mohallem NDS, Viana MM, de Jesus MAML, de Magalhães Gomes GH, de Sousa Lima LF et al. Pure and Nanocomposite Thin Films Based on TiO_2 Prepared by Sol-Gel Process: Characterization and Applications. In: Titanium Dioxide-Material for a Sustainable Environment. Intech, 2018.

45. Hernandez JV. Structural and Morphological modification of TiO_2 doped metal ions and investigation of photo-induced charge transfer processes 2017 (Doctoral dissertation, Université du Maine; Instituto politécnico nacional (México)).

46. Oluwabi AT, Juma AO, Oja I, Mere A, Krunks M. Effect of Zr doping on the structural and electrical properties of spray deposited TiO_2 thin films. Journal of Materials Science 2018; 147-157.

47. Sadikin SN, Rahman MYA, Umar AA, Salleh MM. Effect of spin-coating cycle on the properties of TiO_2 thin film and performance of DSSC. International Journal of Electrochemical Science 2017; 12: 5538. doi: 10.20964/2017.06.57

48. Al-Taweel SS, Saud HR. New route for synthesis of pure anatase TiO_2 nanoparticles via utrasound-assisted sol-gel method. Journal of Chemical and Pharmaceutical Research 2016; 8 (2): 620-626.

49. Amirtharajan S, Jeyaprakash P, Natarajan J. Electrical investigation of TiO_2 thin films coated on glass and silicon substrates-effect of UV and visible light illumination. Applied Nanoscience 2016; 6: 591-598. doi: 10.1007/s13204-015-0464-0

50. He J, Du Y, Bai Y, An J, Cai X et al. Nanocomposites with Enhanced Photocatalytic Activity. Molecules 2019; 1-14.

51. Wiatrowski A, Mazur M, Obstarczyk A, Wojcieszak D, Kaczmarek D et al. Comparison of the physicochemical properties of TiO_2 thin films obtained by magnetron sputtering with continuous and pulsed gas flow. Coatings 2018. doi: 10.3390/coatings8110412

52. Choudhury B, Borah B, Choudhury A. Extending photocatalytic activity of TiO_2 nanoparticles to visible region of illumination by doping of cerium. Photochemistry and Photobiology 2012; 257-264. doi: 10.1111/j.1751-1097.2011.01064.x

53. Li S, Wang Q, Chen T, Zhou Z, Wang Y et al. Study on cerium-doped nano-TiO_2 coatings for corrosion protection of 316 L stainless steel. Nanoscale Research Letters 2012; 1-9.

54. Ohsaka T, Izumi F, Fujiki Y. Raman spectrum of anatase, TiO_2. Nanoscale Research Letters 1978; 7: 321-324.

55. Chanda A. Structural and magnetic study of undoped and cobalt doped TiO_2 nanoparticles. RSC Advances 2018; 8: 10939-10947. doi: 10.1039/C8RA00626A

56. Szkoda M, Lisowska-oleksiak A, Siuzdak K. Optimization of boron-doping process of titania nanotubes via electrochemical method toward enhanced photoactivity. Journal of Solid State Electrochemisty 2016; 1765-1774. doi: 10.1007/s10008-016-3185-8

57. Pal M, Pal U, Miguel J, Jiménez GY, Pérez-rodríguez F. Effects of crystallization and dopant concentration on the emission behavior of TiO_2: Eu nanophosphors. Nanoscale Research Letters 2012;7: 1. doi: 10.1186/1556-276X-7-1

58. Pu P, Cachet H, Ngaboyamahina E, Sutter EMM. Relation between morphology and conductivity in TiO_2 nanotube arrays: An electrochemical impedance spectrometric investigation. Journal of Solid State Electrochemistry 2013; 17: 817-828. doi: 10.1007/s10008-012-1931-0

59. Pu P, Cachet H, Sutter EMM. Electrochemical impedance spectroscopy to study photo-induced effects on self-organized TiO_2 nanotube arrays. Electrochimica Acta 2010, 55: 5938-5946. doi: 10.1016/j.electacta.2010.05.048

60. Kawde A, Annamalai A, Amidani L, Boniolo M, Kwong WL et al. Sustainable Energy & Fuels Photo-electrochemical hydrogen production from neutral phosphate buffer and seawater using functionalized by solution-based methods. The Royal Society of Chemistry 2018. doi: 10.1039/c8se00291f

61. Govindan. K, Raja M, Maheshwari SU, Noel M. Analysis and understanding of amido black 10B dye degradation in aqueous solution by electrocoagulation with the conventional oxidants peroxomonosulfate, peroxodisulfate and hydrogen peroxide. Environmental Science: Water Research and Technology 2014. doi: 10.1039/C4EW00030G

62. Amala J, Joice I, Sivakumar T, Ramakrishnan R, Ramya G, Pillai K et al. Visible active metal decorated titania catalysts for the photocatalytic degradation of Amidoblack-10B. Chemical Engineering Journal 2012; 210: 385-397. doi: 10.1016/j.cej.2012.08.103

63. Kashyap J, Ashraf SM, Riaz U. Highly efficient photocatalytic degradation of amido black 10B dye using polycarbazole-decorated TiO_2 nanohybrids. ACS Omega 2017; doi: 10.1021/acsomega.7b01154

64. Trovo AG, Hassan AK, Sillanpaa M, Tang WZ. Degradation of acid blue 161 by fenton and photo-fenton processes. International Journal of Environmental Science and Technology 2016; 147-158. doi: 10.1007/s13762-015-0854-6

65. Li FB, Li XZ, Hou MF, Cheah KW, Choy WCH. Enhanced photocatalytic activity of Ce^{3+}– TiO_2 for 2-mercaptobenzothiazole degradation in aqueous suspension for odour control. Applied Catalysis A: General 2005; 285: 181-189. doi: 10.1016/j.apcata.2005.02.025

66. Gabriela Bonfanti V, Humberto JJ, Michael P, Vanessa Zanon B, Pedro AM. Regina De Fatima Peralta Muniz, CeO_2/TiO_2 nanostructures enhance adsorption and photocatalytic degradation of organic compounds in aqueous suspension. Journal of Photochemistry and Photobiology: A: Chemistry 2017. doi: 10.1016/j.jphotochem.2017.11.045

67. Xie Y, Yuan C, Li X. Photosensitized and photocatalyzed degradation of azo dye using Ln^{n+}-TiO_2 sol in aqueous solution under visible light irradiation. Materila Sicence and Engineering B 2005; 117: 325–333. doi: 10.1016/j.mseb.2004.12.073

68. Kumar A, Pandey G. A review on the factors affecting the photocatalytic degradation of hazardous materials. Material Science and Engineering: International Journal 2017; 106-114. doi: 10.15406/mseij.2017.01.00018

69. Rauf MA, Meetani MA, Hisaindee S. An overview on the photocatalytic degradation of azo dyes in the presence of TiO_2 doped with selective transition metals. Desalination 2011; 276: 13-27.doi: 10.1016/j.desal.2011.03.071

70. Gupta VK, Jain R, Nayak A, Agarwal S, Shrivastava M. Removal of the hazardous dye — Tartrazine by photodegradation on titanium dioxide surface. Material Science and Engineering: C 2011; 31: 1062-1067. doi: 10.1016/j.msec.2011.03.006

71. Ferkous H, Hamdaoui O, Merouani S. Sonochemical degradation of naphthol blue black in water: effect of operating parameters. Ultrasonics Sonochemistry 2015. doi: 10.1016/j.ultsonch.2015.03.013

72. Abhishek G, Munish M, Vijaya KB, Barman S. Experimental investigation on adsorption of amido black 10B dye onto zeolite synthesized from fly ash. Chemical Engineering Communications 2015; 37-41. doi: 10.1080/00986445.2013.836636

73. Ajmal A, Majeed I, Malik N. Principles and mechanisms of photocatalytic dye degradation on TiO_2 based photocatalysts: a comparative overview. RSC Advances 2014; 37003-37026. doi: 10.1039/C4RA06658H

74. Mamun K, Asw R, Fahmida K. Parameters affecting the photocatalytic degradation of dyes using TiO_2: A review. Applied Water Science 2017; 7: 1569-1578. doi: 10.1007/s13201-015-0367-y

75. Akpan UG, Hameed BH. Parameters affecting the photocatalytic degradation of dyes using TiO_2-based photocatalysts: A review. Journal of Hazardous Materials 2009; 170: 520-529. doi: 10.1016/j.jhazmat.2009.05.039

76. Meetani MA, Hisaindee SM, Abdullah F, Ashraf SS, Rauf MA. Liquid chromatography tandem mass spectrometry analysis of photodegradation of a diazo compound : A mechanistic study. Chemosphere 2010; 80422-427. doi: 10.1016/j.chemosphere.2010.04.065